Programming Colloidal Crystal Habit with Anisotropic Nanoparticle Building Blocks and DNA Bonds

Matthew N. O'Brien,[†,§] Hai-Xin Lin,[†,§] Martin Girard,[‡] Monica Olvera de la Cruz,[†,‡] and Chad A. Mirkin*[,†,‡]

[†]Department of Chemistry, International Institute for Nanotechnology, Northwestern University, Evanston, Illinois 60208, United States

[‡]Department of Materials Science and Engineering, Northwestern University, Evanston, Illinois 60208, United States

Ⓢ *Supporting Information*

ABSTRACT: Colloidal crystallization can be programmed using building blocks consisting of a nanoparticle core and DNA bonds to form materials with controlled crystal symmetry, lattice parameters, stoichiometry, and dimensionality. Despite this diversity of colloidal crystal structures, only spherical nanoparticles crystallized with BCC symmetry experimentally yield single crystals with well-defined crystal habits. Here, we use low-symmetry, anisotropic nanoparticles to overcome this limitation and to access single crystals with different equilibrium Wulff shapes: a cubic habit from cube-shaped nanoparticles, a rhombic dodecahedron habit from octahedron-shaped nanoparticles, and an octahedron habit from rhombic dodecahedron-shaped nanoparticles. The observation that one can control the microscopic shape of single crystals based upon control of particle building block and crystal symmetry has important fundamental and technological implications for this novel class of colloidal matter.

The equilibrium shape of a crystal can be predicted with a Wulff construction, which plots the surface energy (γ) along each direction of a crystalline lattice in order to identify local minima in γ.[1−3] The crystalline planes corresponding to these minima possess the most stable interactions, and thus one would expect crystals bound by these facets. However, experimental realization of equilibrium structures represents a significant challenge in many atomic, molecular, and nanoscale systems due to energetic fluctuations in the system greater than the differences in γ. In the context of DNA-mediated nanoparticle crystallization, the most stable interactions often contain the greatest number of hybridization events, or "bonding" interactions, between the DNA ligands on neighboring particles.[4−11] Control of crystal habit therefore relates to the relative number of hybridization events along different crystalline planes,[12] which can be tuned based on nanoparticle size and shape, DNA length and density, and lattice symmetry.[13−18] Despite their widespread use, high symmetry spherical nanoparticles are particularly challenging building blocks to use in this endeavor. This challenge originates from the weak interaction strength between spheres along their curved surfaces, as evidenced by relatively low DNA dehybridization temperatures (T_m)[19,20] and small fractions of

hybridized DNA, and the rotational freedom of spheres within a lattice.[12,21] In contrast, the reduced symmetry of polyhedral nanoparticles yields structures that can template an oriented array of densely packed DNA on each facet, which facilitates stronger, directional interactions. Recent work has introduced the concept of a "zone of anisotropy" for polyhedral nanoparticles, or the phase space where directional interactions templated by the anisotropy of the particle core persist and result in correlated particle orientations.[11,13,15,16,19,20] Importantly, the face-to-face interactions that occur within this zone of anisotropy possess greater fractions of hybridized DNA and greater rotational restrictions than spherical nanoparticles, which in principle, should enable experimental realization of equilibrium habits (Figure 1).

To test this hypothesis, three different polyhedral nanoparticle shapes were investigated: cubes, octahedra, and rhombic dodecahedra (Figure 1).[16,22] When particles are prepared with self-complementary DNA sequences, such that
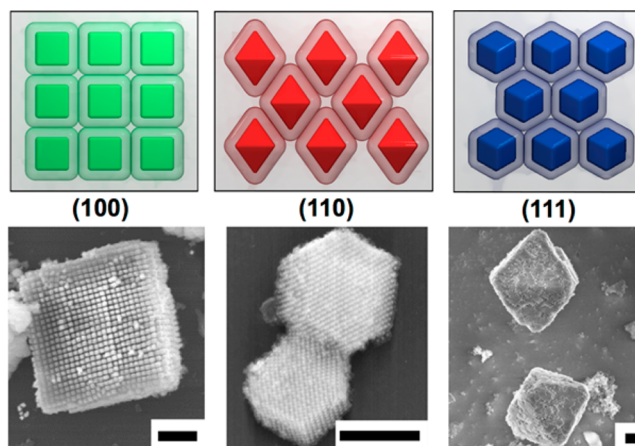

Figure 1. Nanoparticle shape can be used to control crystal habit in DNA-mediated nanoparticle crystallization. Each shape crystallizes into a lattice with a different closest-packed plane (top) and crystal habit (bottom). Cube, octahedron, and rhombic dodecahedron nanoparticles (left to right) are shown with cube, rhombic dodecahedron, and octahedron crystal habits, respectively. Scale bars: 1 μm.
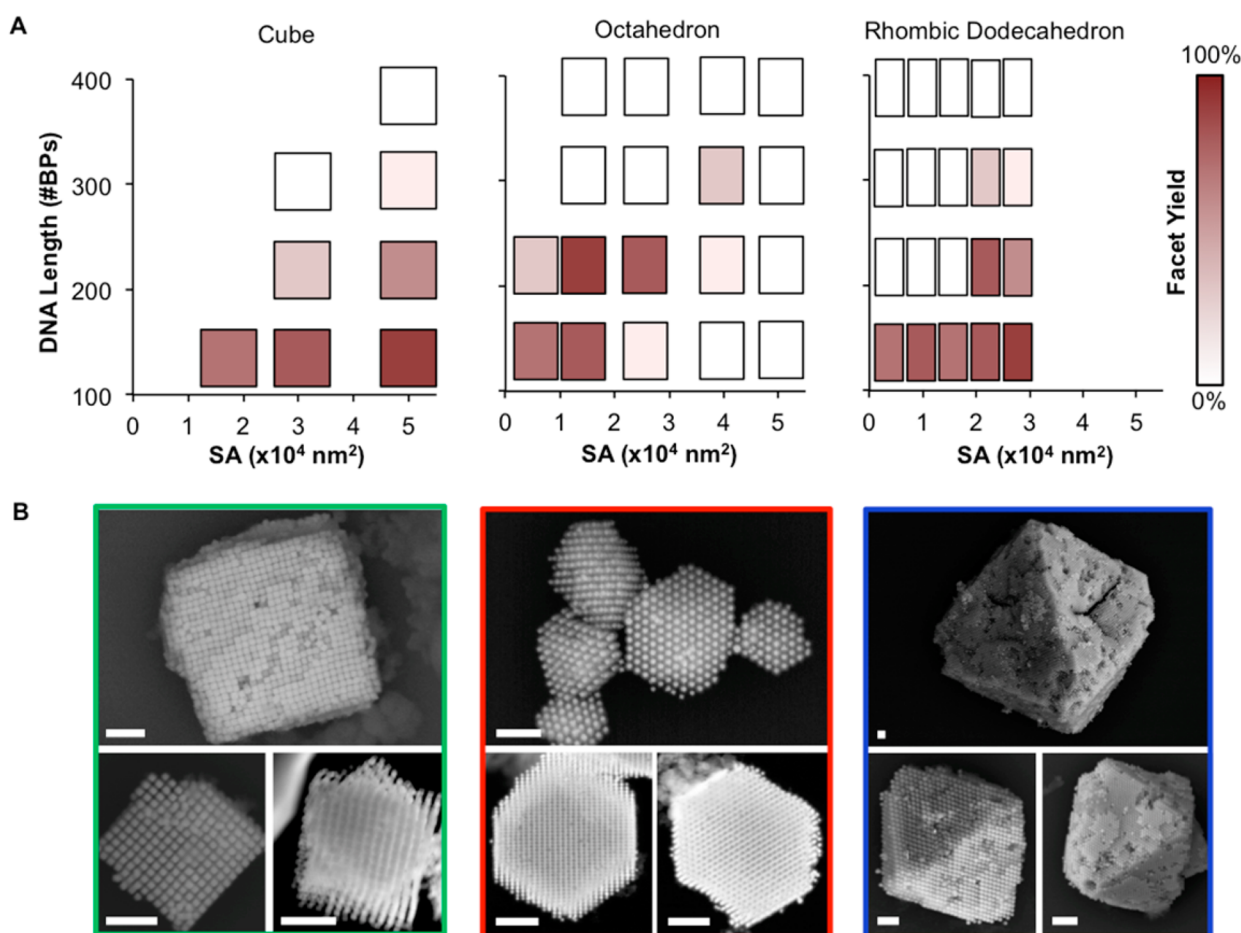
Figure 2. Yield of crystals with equilibrium facets can be controlled based on particle symmetry, particle size (shown here as surface area, SA), and DNA length (*D*). (A) Facet yields are plotted over the phase space encoded by SA and *D* for each shape, where yield is color-coded and determined from EM analysis of silica-embedded crystals. (B) Examples of the highest quality crystals formed from the investigated phase space, all with the predicted Wulff shape. Scale bars: 500 nm.

every particle can connect to its neighbors, each of these shapes should crystallize into lattice symmetries with different closest packed planes and thus different Wulff shapes.[16] Within the zone of anisotropy for each shape, one would expect that cubes should crystallize into lattices with simple cubic (SC) symmetry, {100} closest packed planes, and cube habits; octahedra should crystallize into lattices with BCC symmetry, {110} closest packed planes, and rhombic dodecahedron habits; and rhombic dodecahedra should crystallize into lattices with face-centered cubic (FCC) symmetry, {111} closest packed planes, and truncated octahedron habits. Indeed, the expected crystal habits can be experimentally realized with careful control of the crystallization conditions (Figure 1).

Two recent advances are of particular importance to realize these structures. First, advances in seed-mediated nanoparticle synthesis enable the use of significantly more uniform building blocks (>95% shape yield with <5% variation in size),[22] compared to previous investigations.[13] This uniformity minimizes inhomogeneity-related microstrain and kinetic traps that impede well-defined habits.[11,15,23] Second, a recently reported slow-annealing process enables fine control of crystallization conditions.[12] The temperature gradient of this process controls whether the system reaches equilibrium at each temperature, and thus the slow rates achievable in this process enable access to equilibrium habits.[11,12]

Given these results, it was hypothesized that crystal yield could be controlled via particle surface area (SA) and DNA length (*D*) and predicted by the experimentally elucidated zone of anisotropy for each shape. Specifically, as SA increases for a given particle shape (for a fixed *D*), the number of DNA strands per facet increases. This structural change should result in a greater number of hybridization events between facets, a more stable interaction, and therefore an increased crystal yield. Alternatively, as *D* increases (for a fixed SA), the DNA shell should lose the directional interactions templated by the particle core, and in turn, decrease the fraction of hybridized DNA, the stability of the interaction, and the crystal yield.[16] Thus, crystal yields would be predicted to improve with large SA and small *D*.

To characterize habit, crystals were transferred to the solid state via silica encapsulation and subsequently imaged by electron microscopy (EM). Although EM analysis suffers from sampling bias that limits the quantitative description of the crystal population, this method provides the most direct insight into microstructure. Two separate yield calculations were done by EM analysis to better understand trends in SA and *D*: (1) Facet yield, the yield of crystalline domains with equilibrium facets; and (2) Habit yield, the yield of discrete single crystals with the expected habit (Figure S1; Tables S1−S2). Facet yield captures how favorable the growth conditions are for the

expected facet, while the habit yield additionally factors in nucleation and sample preparation effects.

For the cube and rhombic dodecahedron samples, indeed, both the facet and habit yields increased with SA and decreased with D, consistent with predictions (Figure 2; Figures S2−S6, S11−S14). At the largest values of SA and smallest values of D investigated, this resulted in facet yields of 85 and 93%, and habit yields of 79 and 77% for cubes and rhombic dodecahedra, respectively (Figure 2A). It is worth noting that spherical nanoparticles assembled with these symmetries (SC and FCC) via similar methods do not result in crystals with well-defined habits, which is consistent with the central hypothesis of this work.[12] Octahedra, however, possess a more complicated trend in yields that depends on the relative ratio of SA and D, wherein the highest yields are achieved for intermediate values (Figure 2A; Figures S7−S10). This deviation can be understood based on the competition between the dense packing behavior of octahedra based on geometric considerations[24−26] and the maximization of DNA hybridization events via face-to-face interactions.[13,16] The relative ratio between SA and D necessary to observe equilibrium habits likely reflects the hydrodynamic truncation (due to the DNA shell) where the geometric and DNA driving forces both favor BCC symmetry.

Outside of the phase space investigated here, transitions in the lattice symmetry can occur, which would favor different crystal habits.[16] In particular, experimental investigation of cubes assembled into a body-centered tetragonal (BCT) lattice form an elongated rhombic dodecahedron habit for short D and small SA, consistent with the Wulff construction for that symmetry (Figure S15). BCT crystals can be stabilized over an even wider range of conditions at elevated salt concentrations, as the decreased electrostatic repulsion between DNA strands results in more flexible DNA, and thus a smaller zone of anisotropy (Figure S16). This observation opens up an exciting possibility to use the same nanoparticle shape to access different macroscopic crystal habits and therefore merits further investigation.

To corroborate these results, these systems were modeled with MD simulations using the HOOMD package,[27,28] previously shown to describe accurately crystallization behavior.[16,21] In particular, γ was calculated with a broken-bond model that only considers nearest neighbor contributions, wherein a crystal is cut along different crystalline planes to expose or "break" bonds between particles (Figure S17).[2,3,29] γ represents the excess energy at the exposed surface (per unit area) relative to the bulk, and the more stable the interaction, the lower the γ. The ratio of γ along different planes can then be used to determine the favorability of a particular facet and crystal habit. Here, the surface enthalpy portion of γ is extracted from simulations, analogous to literature precedent, due to challenges associated with surface entropy measurements (see SI Discussion). Importantly, these surface enthalpy ratios predict the experimentally observed closest-packed planes, and match well with an idealized broken bond model that scales surface enthalpy with the exposed SA (Table S3). These simulated values match nearly identically for the cube and rhombic dodecahedron nanoparticle systems. For octahedra, these surface enthalpy ratios approach the broken bond model for large L; at small L, deviations occur due to second nearest neighbor interactions between vertices (Table S3). When surface enthalpy values are used in Wulff constructions, we also recreate similar crystal habits as those observed experimentally (Figure S18A,B). Interestingly, for the crystals formed from

rhombic dodecahedra, we observe less truncation than predicted from surface enthalpy calculations (Figure S18), which suggests that surface entropy may play a significant role in this particular system.

Although defined crystal shapes can be accessed via other nanoparticle assembly methods, the predictive power of DNA-programmable interactions uniquely allows habit to be designed prior to experiments, rather than after a complex rationalization of the many driving forces involved. Looking forward, these results suggest that several additional habits can likely be realized with advances in nanoparticle synthesis, the use of molecularly defined cages,[30−32] or asymmetric functionalization[33] toward the construction of a greater library of crystal habits. This library will enable researchers to probe the interplay between nanoscale and mesoscale structure on the optoelectronic, magnetic, catalytic, and mechanical properties of these materials.[34,35] Moreover, they will allow one to manipulate these "supercrystals" as individual devices or as building blocks for hierarchical organization.[11]

■ ASSOCIATED CONTENT

ⓢ Supporting Information

The Supporting Information is available free of charge on the ACS Publications Web site at DOI: 10.1021/jacs.6b09704.

Methods and materials, additional electron microscopy images, crystal yields, and molecular dynamics simulations (PDF)

■ AUTHOR INFORMATION

Corresponding Author

*chadnano@northwestern.edu

Author Contributions

§These authors contributed equally.

Notes

The authors declare no competing financial interest.

■ REFERENCES

(1) Wulff, G. *Z. Kristallogr. - Cryst. Mater.* **1901**, 34, 449.
(2) Markov, I. V. *Crystal Growth for Beginners: Fundamentals of Nucleation, Crystal Growth and Epitaxy*; 2nd ed.; World Scientific: River Edge, NJ, 2003.
(3) Fredriksson, H.; Akerlind, U. *Solidification and Crystallization Processing in Metals and Alloys*; Wiley: Hoboken, NJ, 2012.

(4) Mirkin, C. A.; Letsinger, R. L.; Mucic, R. C.; Storhoff, J. J. *Nature* **1996**, *382*, 607.

(5) Alivisatos, A. P.; Johnsson, K. P.; Peng, X. G.; Wilson, T. E.; Loweth, C. J.; Bruchez, M. P.; Schultz, P. G. *Nature* **1996**, *382*, 609.

(6) Macfarlane, R. J.; O'Brien, M. N.; Petrosko, S. H.; Mirkin, C. A. *Angew. Chem., Int. Ed.* **2013**, *52*, 5688.

(7) Michele, L. D.; Eiser, E. *Phys. Chem. Chem. Phys.* **2013**, *15*, 3115.

(8) Jones, M. R.; Seeman, N. C.; Mirkin, C. A. *Science* **2015**, *347*, 1260901.

(9) Zhang, X.; Wang, R.; Xue, G. *Soft Matter* **2015**, *11*, 1862.

(10) Rogers, W. B.; Shih, W. M.; Manoharan, V. N. *Nat. Rev. Mater.* **2016**, *1*, 16008.

(11) O'Brien, M. N.; Jones, M. R.; Mirkin, C. A. *Proc. Natl. Acad. Sci. U. S. A.* **2016**, *113*, 11717.

(12) Auyeung, E.; Li, T. I. N. G.; Senesi, A. J.; Schmucker, A. L.; Pals, B. C.; de la Cruz, M. O.; Mirkin, C. A. *Nature* **2014**, *505*, 73.

(13) Jones, M. R.; Macfarlane, R. J.; Lee, B.; Zhang, J.; Young, K. L.; Senesi, A. J.; Mirkin, C. A. *Nat. Mater.* **2010**, *9*, 913.

(14) Macfarlane, R. J.; Lee, B.; Jones, M. R.; Harris, N.; Schatz, G. C.; Mirkin, C. A. *Science* **2011**, *334*, 204.

(15) O'Brien, M. N.; Jones, M. R.; Lee, B.; Mirkin, C. A. *Nat. Mater.* **2015**, *14*, 833.

(16) O'Brien, M. N.; Girard, M.; Lin, H.-X.; Millan, J. A.; Olvera de la Cruz, M.; Lee, B.; Mirkin, C. A. *Proc. Natl. Acad. Sci. U. S. A.* **2016**, *113*, 10485.

(17) Wang, Y.; Wang, Y.; Zheng, X.; Ducrot, E.; Yodh, J. S.; Weck, M.; Pine, D. J. *Nat. Commun.* **2015**, *6*, 7253.

(18) Macfarlane, R. J.; Jones, M. R.; Lee, B.; Auyeung, E.; Mirkin, C. A. *Science* **2013**, *341*, 1222.

(19) Jones, M. R.; Macfarlane, R. J.; Prigodich, A. E.; Patel, P. C.; Mirkin, C. A. *J. Am. Chem. Soc.* **2011**, *133*, 18865.

(20) O'Brien, M. N.; Brown, K. A.; Mirkin, C. A. *ACS Nano* **2016**, *10*, 1363.

(21) Li, T. I. N. G.; Sknepnek, R.; Macfarlane, R. J.; Mirkin, C. A.; Olvera de la Cruz, M. *Nano Lett.* **2012**, *12*, 2509.

(22) O'Brien, M. N.; Jones, M. R.; Brown, K. A.; Mirkin, C. A. *J. Am. Chem. Soc.* **2014**, *136*, 7603.

(23) Auer, S.; Frenkel, D. *Nature* **2001**, *413*, 711.

(24) Agarwal, U.; Escobedo, F. A. *Nat. Mater.* **2011**, *10*, 230.

(25) Henzie, J.; Grünwald, M.; Widmer-Cooper, A.; Geissler, P. L.; Yang, P. *Nat. Mater.* **2012**, *11*, 131.

(26) Gantapara, A. P.; de Graaf, J.; van Roij, R.; Dijkstra, M. *Phys. Rev. Lett.* **2013**, *111*, 015501.

(27) Anderson, J. A.; Lorenz, C. D.; Travesset, A. *J. Comput. Phys.* **2008**, *227*, 5342.

(28) Glaser, J.; Nguyen, T. D.; Anderson, J. A.; Lui, P.; Spiga, F.; Millan, J. A.; Morse, D. C.; Glotzer, S. C. *Comput. Phys. Commun.* **2015**, *192*, 97.

(29) Mackenzie, J. K.; Moore, A. J. W.; Nicholas, J. F. *J. Phys. Chem. Solids* **1962**, *23*, 185.

(30) Kuzyk, A.; Schreiber, R.; Fan, Z.; Pardatscher, G.; Roller, E.-M.; Hogele, A.; Simmel, F. C.; Govorov, A. O.; Liedl, T. *Nature* **2012**, *483*, 311.

(31) Liu, W.; Tagawa, M.; Xin, H. L.; Wang, T.; Emamy, H.; Li, H.; Yager, K. G.; Starr, F. W.; Tkachenko, A. V.; Gang, O. *Science* **2016**, *351*, 582.

(32) Tian, Y.; Zhang, Y.; Wang, T.; Xin, H. L.; Li, H.; Gang, O. *Nat. Mater.* **2016**, *15*, 654.

(33) Halverson, J. D.; Tkachenko, A. V. *Phys. Rev. E* **2013**, *87*, 062310.

(34) Park, D. J.; Zhang, C.; Ku, J. C.; Zhou, Y.; Schatz, G. C.; Mirkin, C. A. *Proc. Natl. Acad. Sci. U. S. A.* **2015**, *112*, 977.

(35) Ross, M. B.; Ku, J. C.; Vaccarezza, V. M.; Schatz, G. C.; Mirkin, C. A. *Nat. Nanotechnol.* **2015**, *10*, 453.